Search for Antideuterons of Cosmic Origin
Using the BESS-Polar II Magnetic-Rigidity Spectrometer

K. Sakai[1,2,*] H. Fuke[3] K. Yoshimura,[4] M. Sasaki[1,2] K. Abe,[5,‡] S. Haino,[6,§] T. Hams,[1,2] M. Hasegawa[6]
K. C. Kim[7] M. H. Lee[7,‖] Y. Makida,[6] J. W. Mitchell,[1] J. Nishimura,[3,8] M. Nozaki[6] R. Orito,[5,¶]
J. F. Ormes[9] E. S. Seo[7] R. E. Streitmatter,[1,†] N. Thakur,[1,**] A. Yamamoto[6] and T. Yoshida[3]

(BESS Collaboration)

[1]*NASA-Goddard Space Flight Center (NASA-GSFC), Greenbelt, Maryland 20771, USA*
[2]*Center for Research and Exploration in Space Science and Technology (CRESST)*
[3]*Institute of Space and Astronautical Science, Japan Aerospace Exploration Agency (ISAS/JAXA),*
Sagamihara, Kanagawa 252-5210, Japan
[4]*Okayama University, Okayama, Okayama 700-8530, Japan*
[5]*Kobe University, Kobe, Hyogo 657-8501, Japan*
[6]*High Energy Accelerator Research Organization (KEK), Tsukuba, Ibaraki 305-0801, Japan*
[7]*IPST, University of Maryland, College Park, Maryland 20742, USA*
[8]*The University of Tokyo, Bunkyo, Tokyo 113-0033, Japan*
[9]*University of Denver, Denver, Colorado 80208, USA*

We searched for antideuterons ($\bar{d}$'s) in the 4.7×10^9 cosmic-ray events observed during the BESS-Polar II flight at solar minimum in 2007–2008 but found no candidates. The resulting 95% C.L. upper limit on the $\bar{d}$ flux is 6.7×10^{-5} $(\text{m}^2 \, \text{s} \, \text{sr} \, \text{GeV/n})^{-1}$ in an energy range from 0.163 to 1.100 GeV/n. The result has improved by more than a factor of 14 from the upper limit of BESS97, which had a potential comparable to that of BESS-Polar II in the search for cosmic-origin $\bar{d}$'s and was conducted during the former solar minimum. The upper limit of $\bar{d}$ flux from BESS-Polar II is the first result achieving the sensitivity to constrain the latest theoretical predictions.

The cosmic-ray antinuclei, including antiproton ($\bar{p}$), antihelium ($\overline{\text{He}}$), and antideuteron ($\bar{d}$), are essential for understanding the early universe and are unique probes that are sensitive to dark matter (DM) [1,2] and local primordial black holes (PBHs) [3–5] beyond the standard model.

Precise measurements of the $\bar{p}$ fluxes were performed during the BESS-Polar II flight that detected about 8000 $\bar{p}$'s in an energy range from 0.17 to 3.5 GeV [6], while PAMELA detected about 1500 events from 0.06 to 180 GeV [7]. The $\bar{p}$ fluxes calculated in both experiments agree with each other within overall statistical and systematic errors. They are also consistent with the $\bar{p}$'s being of secondary origin, limiting the primary $\bar{p}$'s from PBHs and other sources below the 2 GeV peak suggested by the BESS95 + 97 results [8]. In a higher rigidity region from 1 to 450 GV, a high-statistics $\bar{p}$ flux of 3.49×10^5 events was reported from AMS-02 [9]. The AMS-02 results indicate a possible excess compatible with DM having a mass of 20 to 80 GeV, while it is also consistent with expectations from secondary production within theoretical error. Consequently, in the energy range where measurements have been made, significant improvements in statistical and systematic errors are essential to identify the primary $\bar{p}$'s due to the large background of secondary $\bar{p}$'s.

In contrast to high-statistics $\bar{p}$ measurements, no cosmic-ray $\overline{\text{He}}$ and $\bar{d}$ have been detected [10], as discussed below. Various experiments have been extensively searching for $\overline{\text{He}}$ [11,12], but clear evidences and results are still to be reported. Consequently, a series of BESS flights has resulted in the most stringent upper limit of 1.0×10^{-7} to the ratio $\overline{\text{He}}/\text{He}$ in the rigidity range from 1.6 to 14 GV [13].

An advantage of the $\bar{d}$ search over the $\bar{p}$ measurement lies in the extremely low astrophysical background of $\bar{d}$'s, especially at low energy. In the process of secondary particle production by the interaction of cosmic rays with interstellar gas, the energy threshold of $\bar{d}$ production is higher, and the energy spectrum of cosmic rays is steep, so the calculated secondary $\bar{d}$ flux peaks above a few GeV/n. Various DM and PBH models constrained by the $\bar{p}$ measurements predict primary $\bar{d}$ fluxes that exceed the secondary background by 2 to 3 orders of magnitude below around 1 GeV/n at solar minimum [1,14]. A large enhancement is predicted to emerge in the low-energy

cosmic-origin $\bar{d}$'s at solar minimum, while there is no significant variation in the astrophysical background, making the solar minimum phase the most suitable period to search for primary $\bar{d}$'s. Four BESS balloon flights in 1997 through 2000 determined an upper limit of 9.8×10^{-4} $(m^2 \, s \, sr \, GeV/n)^{-1}$ on the $\bar{d}$ flux at solar minimum in 1997 and an upper limit of 1.9×10^{-4} $(m^2 \, s \, sr \, GeV/n)^{-1}$ on the integrated $\bar{d}$ flux for the four flights in the energy range from 0.170 to 1.150 GeV/n [3]. The BESS97-00 result, including the post-solar-minimum observation, realized the best sensitivity to the search for cosmic-origin $\bar{d}$'s prior to BESS-Polar II.

The sensitivity of experiments searching for $\bar{d}$'s is expected to grow significantly in the next few years. AMS-02 stated that the next frontier would be searches for $\bar{d}$, $\overline{He}$, and heavier antinuclei [12]. GAPS will conduct a series of long duration balloon (LDB) flights over Antarctica to search for low-energy $\bar{d}$'s below 0.25 GeV/n [15]. Future experiments such as GRAMS [16] and ADHD [10] will come in the next few decades. One of the reasons for the growing interest in detecting cosmic-ray $\bar{d}$'s is the availability of accelerator data on $\bar{d}$ formation [17]. In particular, the recent pp collider results, by ALICE [18,19], are entirely identical to the production process of the astrophysical background, contributing significantly to the accuracy of the secondary $\bar{d}$ flux calculations. This paper reports on the $\bar{d}$ search with BESS-Polar II, performed at the solar minimum in 2007–2008, before the next generation experiments to be realized.

The concept of BESS-Polar II, the successor to BESS [20–23] and BESS-Polar I [24–26], was to realize high-statistics observations of low-energy $\bar{p}$ events made available by a thin superconducting solenoid at solar minimum by using a high-resolution magnetic-rigidity spectrometer with a large geometrical acceptance of 0.23 m^2 sr and an LDB flight over Antarctica. BESS-Polar II was launched on December 23, 2007, and observed cosmic rays for 24.5 days with the spectrometer magnet kept energized at 34 to 38 km (average overburden of 5.81 g/cm^2) and a cutoff rigidity below 0.5 GV, accumulating 13.6 terabytes of data, and recording 4.7×10^9 events [27].

The magnetic field was stably kept at 0.8 T, with a sufficient operational margin compared to the maximum field of 1 T. The uniform magnetic field area was filled with a JET-type drift chamber (JET) with nearly no material in the tracking volume, other than pure CO_2 gas, and Inner drift chambers (IDCs) with two tracking layers each are located above and below the JET. Tracking was performed by fitting up to 52 hit points with a characteristic resolution of ~140 μm in the bending plane, resulting in the deflection resolution $[\sigma(R^{-1})]$ of 4.2 TV^{-1} for tracks with the longest possible lengths in the spectrometer corresponding to a maximum detectable rigidity (MDR) of 240 GV. Upper and lower scintillator hodoscopes provided time-of-flight

(TOF) and dE/dx measurements and the event trigger. The timing resolution of the TOF system was 120 ps, giving a β^{-1} resolution of 2.5%. The instrument also incorporated a threshold-type Cherenkov counters (ACC) using a silica aerogel radiator with the refractive index $n = 1.03$ rejecting e^- and μ^- backgrounds by a factor of 17 700 and distinguishing $\bar{d}$'s from such backgrounds up to 3.0 GeV/n. In $\bar{d}$ analysis, $\bar{p}$'s are the majority of backgrounds, rather than the light particles that the ACC vetoes.

$\bar{d}$ candidates require interaction-free and high-quality measurements. Deuteron (d) candidates with the same selection criteria are obtained to determine the selection efficiencies assuming that the noninteracted $\bar{d}$ process is identical to the noninteracted d process. The cuts for $\bar{d}$ selection are similar to $\bar{p}$ cut criteria [6] except for the veto of noisy IDC events, strict fiducial cut for selecting the particle that passes through the JET center region, and applying the ACC veto to the all energy ranges instead of only higher velocity particles with $\beta\gamma$ above 1.56. Since this analysis is the detection study of $\bar{d}$'s, we employed a slightly tighter cut to minimize the risk of misidentification, such as a $\bar{p}$ mimicking a $\bar{d}$.

The search for $\bar{d}$'s was performed by particle identification using $(dE/dx)^{0.5}$ versus rigidity and β^{-1} versus rigidity. Figure 1 shows the $(dE/dx)^{0.5}$ versus rigidity at the upper and lower TOF counter and JET chamber. Solid line bands denote the d and $\bar{d}$ selection. An updated TOF
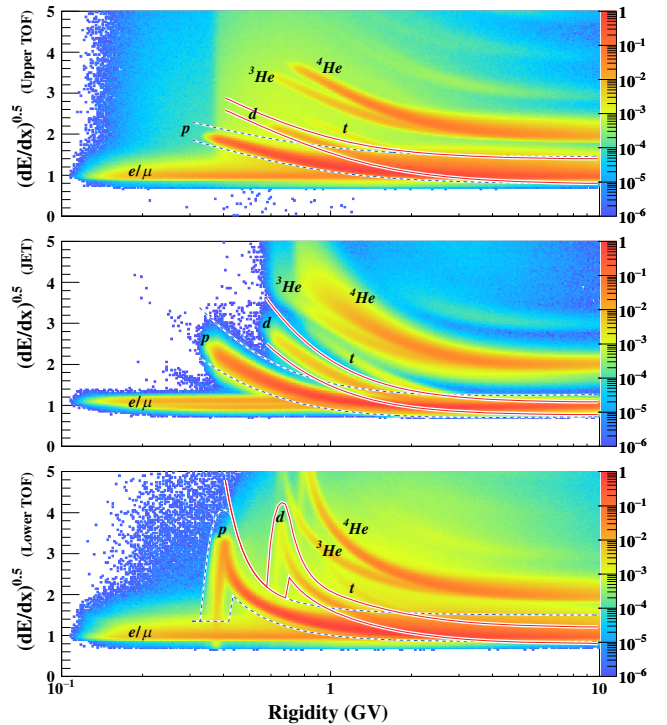

FIG. 1. d's ($\bar{d}$'s) and p's ($\bar{p}$'s) bands in $(dE/dx)^{0.5}$ versus rigidity at the magnet's center (top: Upper TOF, middle: JET, bottom: Lower TOF) from BESS-Polar II.

calibration improved the charge resolution, resulting in a clearer overall picture and demonstrating a sharp distinction between ^{3}He and ^{4}He, which was previously obscured.

The β^{-1} versus rigidity plot after dE/dx selection for $|Z| = 1$ and Cherenkov veto is shown in Fig. 2. Using high-statistics proton (p) and d, we determined a solid line band with a width of 3.0σ for $\bar{d}$'s and a dashed line band with a width of 3.5σ for $\bar{p}$'s. The $\bar{d}$ identification region was defined by excluding the overlap area of the $\bar{p}$ band from the $\bar{d}$ band. No $\bar{d}$ was identified over the whole energy range. Some events outside the $\bar{d}$ identification region near the boundary look superficially promising; however, all these events distribute only in a higher rigidity region where particle identification is difficult, which are considered to be tail components of $\bar{p}$'s. The event reduction by excluding the $\bar{p}$ β band overlap from the identification region of $\bar{d}$'s was considered as the β band efficiency, and the possible contamination of $\bar{p}$'s was treated as backgrounds. As the β^{-1} distribution of p's and that of $\bar{p}$'s agreed within errors, the β^{-1} tail component, essential for background estimation, was calculated by fitting the β^{-1} histogram of p's with a function based on the Crystal Ball function [28]. Each $\bar{p}$ was weighted by the ratio of the integration of the $\bar{p}$ center region to that of the $\bar{d}$ signal region in the probability density function extracted from p's, and accumulated over the rigidity range. The total number of background events contaminating the $\bar{d}$'s is 2.59. The 95% C.L. upper limit would equal 3.00 for any
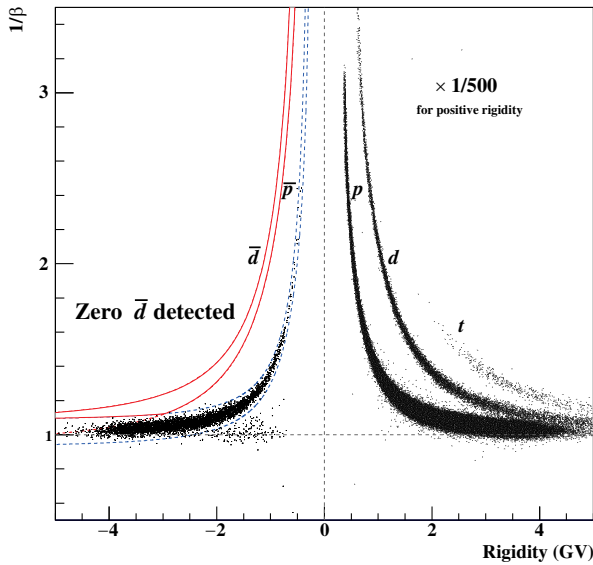

FIG. 2. β^{-1} versus rigidity plot at the magnet's center after dE/dx selection for $|Z| = 1$ and Cherenkov veto. For clarity, only $1/500$ positive-rigidity events are shown. Most of the e^-/μ^- backgrounds are removed by Cherenkov veto; remaining $\bar{p}$'s appear clearly in the dashed line band. There are no $\bar{d}$'s in the identification region, enclosed by solid lines, defined by excluding the overlapping areas of the $\bar{p}$ band from the $\bar{d}$ band.

backgrounds with no signal if we use a flat prior probability density function in Bayesian statistics [29].

Since no cosmic-ray $\bar{d}$'s were found in the BESS-Polar II flight data, an upper limit on the $\bar{d}$ flux was calculated. The 95% C.L. upper limit on the $\bar{d}$ flux ($\Phi_{\bar{d}}$) is defined by Eq. (1).

$$\Phi_{\bar{d}} = \frac{3.00}{F_{\min}(E_2 - E_1)} \tag{1}$$

$$F_{\min} = S\Omega\, T_{\text{live}}\, \varepsilon_{\text{TOI}}\, \varepsilon_{\text{air}} \tag{2}$$

$$\varepsilon_{\text{TOI}} = \varepsilon_{\text{Q-ID}}\, \varepsilon_{\text{other}}\, \varepsilon_{\text{noint}} \tag{3}$$

where $F_{\min}$, E_1 and E_2 are defined below, $S\Omega$ is the geometrical acceptance, T_{live} is the live period, $\varepsilon_{\text{Q-ID}}$ is the detection efficiency of $\bar{d}$'s, $\varepsilon_{\text{other}}$ accounts for other efficiencies described below, $\varepsilon_{\text{noint}}$ is the noninteraction efficiency, ε_{TOI} is the total efficiency at the top of the instrument, ε_{air} is the survival probability in the residual atmosphere.

The Supplemental Material [30] describes the energy dependency; each term's value at 0.5 GeV/n is noted below. $S\Omega$ is 0.133 m^2 sr. This is the nominal value of 0.23 m^2 sr for $S\Omega$ of the BESS-Polar II instrument multiplied by 80.2% from the TOF selection cut requiring two good photomultipliers at both ends of each paddle, 76.8% from the JET central region cut, and 92.6% from the other fiducial cuts. T_{live} is 1 273 381 seconds, identical to the previous analysis calculating proton and helium fluxes [27]. $\varepsilon_{\text{Q-ID}}$ is 67.7%, which is basically stable. In the energy range above 1.0 GeV/n, the selection efficiency of the β band contained in $\varepsilon_{\text{Q-ID}}$ decreases, determining the high energy end of the effective exposure factor. $\varepsilon_{\text{other}}$ is a scalar quantity of 94.1%, including trigger efficiency, track reconstruction efficiency, and accidental track and hits exclusion efficiencies. $\varepsilon_{\text{noint}}$ and ε_{air} were calculated using FTFP_BERT in Geant4.10.07.p03, with $\varepsilon_{\text{noint}}$ being 69.2% and ε_{air} being 80.6%, respectively.

In calculating the conservative upper limit, we adopted the minimum effective exposure factor ($F_{\min}$) contained in an energy range from the lower-end E_1 to the upper-end E_2 of one bin [3,30]. The calculated E_1 and E_2 that could derive the best upper limit are 0.163 and 1.100 GeV/n, respectively, giving an effective exposure factor of $(4.90 \pm 0.16) \times 10^4$ (m^2 s sr). The combined systematic uncertainty σ_{sys} is 3.26%. The largest contributions to the errors included in σ_{sys} are noninteraction, and atmospheric correction errors. In contrast, atmospheric secondary errors do not contribute because background events are ignored, as discussed above. Only upper uncertainties are used to obtain the most conservative upper limit within the range of systematic errors.

Figure 3 shows the 95% C.L. upper limit on the $\bar{d}$ flux at the top of the atmosphere calculated from BESS-Polar II
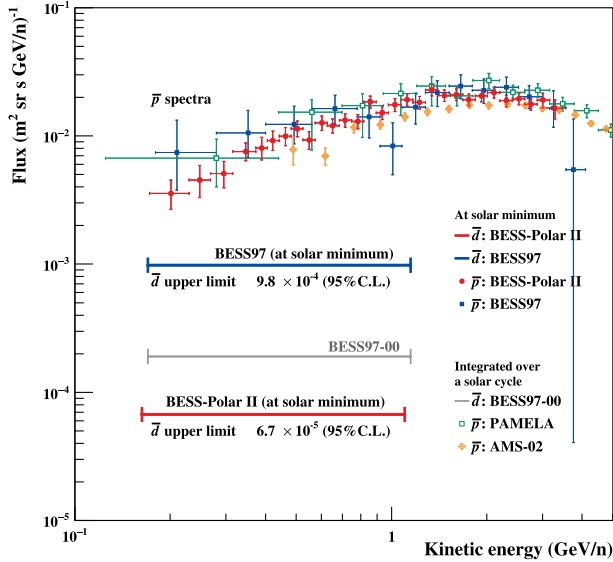
FIG. 3. The upper limit on the $\bar{d}$ flux at the 95% C.L. resulting from BESS-Polar II at solar minimum in 2007–2008, compared with the result from BESS97 at the former solar minimum, as well as the integrated result from BESS97-00 [3]. As references, the antiproton fluxes from BESS97 [8] and BESS-Polar II [6] measured at solar minimum are also shown, as well as the results for PAMELA based on observations from 2006 to 2008 [7] and AMS-02 from 2011 to 2015 [9].

flight data. $\Phi_{\bar{d}}$ is 6.7×10^{-5} $(\mathrm{m^2\,s\,sr\,GeV/n})^{-1}$ in the energy range from 0.163 to 1.100 GeV/n, the most sensitive upper limit on the search for $\bar{d}$'s ever reported. The best upper limit calculated prior to BESS-Polar II was 1.9×10^{-4} $(\mathrm{m^2\,s\,sr\,GeV/n})^{-1}$ on the integrated $\bar{d}$ flux from BESS97-00, which covers half of a solar cycle from solar minimum in 1997 to solar maximum in 2000 [3]. Most currently predicted primary $\bar{d}$ theories have flux shapes that are sensitive to solar modulation, with discovery potentials that drop by 1–2 orders of magnitude from solar minimum to maximum [4]. Hence, the fluxes that are snapshots of the solar minimum are more sensitive to the search for primary $\bar{d}$'s, while the integral flux is superior in having more statistics, although it is complex due to large uncertainties in solar modulation. Furthermore, the searches for $\bar{d}$'s by BESS-Polar II, GAPS, and AMS-02 are complementary since all are optimized at a certain energy and have different systematics from individual instruments and analyses. As the best reference with potential comparable to BESS-Polar II in the search for cosmic-origin $\bar{d}$'s, the upper limit of 9.8×10^{-4} $(\mathrm{m^2\,s\,sr\,GeV/n})^{-1}$ observed by BESS97 at the former solar minimum in 1997 is also shown in Fig. 3. The current result improves the upper limit of BESS97 by more than a factor of 14.

For reference purposes, the upper limits on $\bar{d}$ flux from BESS-Polar II and the solar-minimum $\bar{d}$ flux curves derived from theoretical calculations are shown in Fig. 4. As models for primary $\bar{d}$'s, we refer to the contributions of $b\bar{b}$ DM [1],
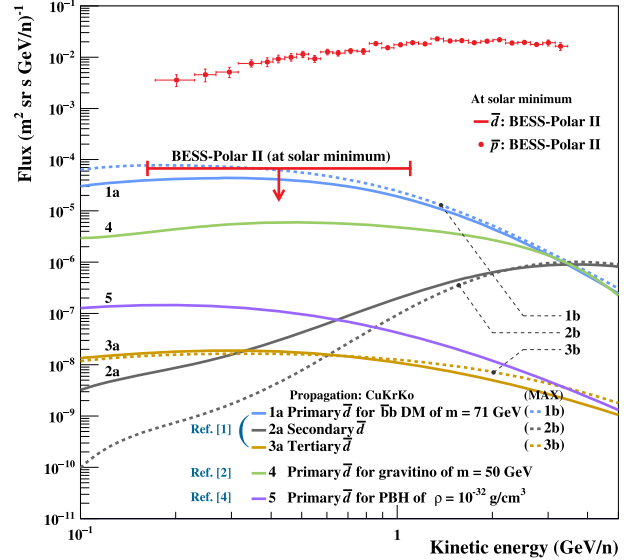

FIG. 4. The upper limit on the $\bar{d}$ flux at the 95% C.L. resulting from BESS-Polar II at solar minimum in 2007–2008, compared with the possible solar-minimum $\bar{d}$ flux curves derived from theoretical calculations. Solid curves (1a, 2a, 3a) and dashed curves (1b, 2b, 3b) calculated with different propagation parameter sets are shown for primary $\bar{d}$'s from $b\bar{b}$ DM, as well as secondary and tertiary contributions, respectively [1]. Solid curves (4, 5) calculated from a single propagation parameter set are presented for theoretically possible primary $\bar{d}$'s from gravitino [2] and PBH [4].

gravitino [2], and PBH [4], as well as calculated $\bar{d}$ fluxes from secondary sources in the interstellar medium and tertiary components that are inelastically scattered secondaries. The theoretical curves for DM origin with a mass of 71 GeV, secondary, and tertiary $\bar{d}$'s [1] are drawn with both a solid line (CuKrKo [31]) and a dashed line (MAX [32]), calculated with different propagation parameters, using a coalescing momentum (p_0) of 248 GeV and solar modulated in the force field approximation with a potential (ϕ) of 400 MV. The solid line for the gravitino origin with a mass of 50 GeV [2] is calculated with the propagation parameter MED, with $p_0 = 143$ GeV and solar modulation of $\phi = 500$ MV MAX and MED are the benchmark scenarios giving maximal and median primary $\bar{p}$ flux [32]. The solid line for the PBH origin with an evaporation rate of 10^{-32} g/cm³ is drawn in the reference [4] as a band with uncertainties from 128.7 to 226.1 MeV for p_0 and from 500 to 1500 MV for ϕ. The upper edge of the band is extracted so that p_0 is 226.1 MeV and ϕ is 500 MV. The propagation parameters are from the model [33]. These show the maximum discovery potential of $\bar{d}$'s at solar minimum for each model, constrained with the boron to carbon flux ratio (B/C) [34], measuring the average amount of interstellar material traversed by cosmic rays, and $\bar{p}$ flux [7,9].

We still need to accept the theoretical uncertainties due to cosmic-ray propagation and solar modulation. A difference

of an order of magnitude in the absolute value of the primary $\bar{d}$ flux between astrophysical parameters MAX and MED in the benchmark scenario, and an inconsistency in solar activity could result in 20%–40% uncertainty between observations with $\phi = 600$ MV and primary $\bar{d}$ calculation at 400, 500 MV. In conclusion, the upper limit on the $\bar{d}$ flux from BESS-Polar II is the first result to achieve the sensitivity to constrain the latest theoretical predictions.

---

[*]Corresponding author: kenichisakai@uchicago.edu
Present address: Enrico Fermi Institute of The University of Chicago, Chicago, Illinois 60637, USA.
[†]Deceased.
[‡]Present address: Kamioka Observatory, Institute for Cosmic Ray Research, The University of Tokyo, Higashi-Mozumi, Kamioka, Hida, Gifu 506-1205, Japan.
[§]Present address: Institute of Physics, Academia Sinica, Nankang, Taipei 11529, Taiwan.
[‖]Present address: Center for Underground Physics, Institute for Basic Science (IBS), Daejeon 34126, Korea.
[¶]Present address: Tokushima University, Tokushima 770-8506, Japan.
[**]Present address: Prince George's Community College, Largo, Maryland 20774, USA.

[1] M. Korsmeier, F. Donato, and N. Fornengo, Prospects to verify a possible dark matter hint in cosmic antiprotons with antideuterons and antihelium, Phys. Rev. D **97**, 103011 (2018).

[2] L. A. Dal and A. R. Raklev, Antideuteron limits on decaying dark matter with a tuned formation model, Phys. Rev. D **89**, 103504 (2014).

[3] H. Fuke *et al.*, Search for cosmic-ray antideuterons, Phys. Rev. Lett. **95**, 081101 (2005).

[4] J. Herms, A. Ibarra, A. Vittino, and S. Wild, Antideuterons in cosmic rays: sources and discovery potential, J. Cosmol. Astropart. Phys. 02 (2017) 018.

[5] B. Carr, K. Kohri, Y. Sendouda, and J. Yokoyama, Constraints on primordial black holes, Rep. Prog. Phys. **84**, 116902 (2021).

[6] K. Abe *et al.*, Measurement of the cosmic-ray antiproton spectrum at solar minimum with a long-duration balloon flight over Antarctica, Phys. Rev. Lett. **108**, 051102 (2012).

[7] O. Adriani *et al.*, PAMELA results on the cosmic-ray antiproton flux from 60 MeV to 180 GeV in kinetic energy, Phys. Rev. Lett. **105**, 121101 (2010).

[8] S. Orito *et al.*, Precision measurement of cosmic-ray antiproton spectrum, Phys. Rev. Lett. **84**, 1078 (2000).

[9] M. Aguilar *et al.*, Antiproton flux, antiproton-to-proton flux ratio, and properties of elementary particle fluxes in primary cosmic rays measured with the alpha magnetic spectrometer on the international space station, Phys. Rev. Lett. **117**, 091103 (2016).

[10] P. von Doetinchem *et al.*, Cosmic-ray antinuclei as messengers of new physics: status and outlook for the new decade, J. Cosmol. Astropart. Phys. 08 (2020) 035.

[11] A. Kounine, AMS Experiment on the International Space Station, Next generation of AstroParticle experiments in space (NextGAPES-2019) (2019), http://www.sinp.msu.ru/contrib/NextGAPES/files/AMS_AK.pdf.

[12] R. Battiston, High precision cosmic ray physics with AMS-02 on the International Space Station, Riv. Nuovo Cimento **43**, 319 (2020).

[13] K. Abe *et al.*, Search for antihelium with the BESS-polar spectrometer, Phys. Rev. Lett. **108**, 131301 (2012).

[14] F. Donato, N. Fornengo, and P. Salati, Antideuterons as a signature of supersymmetric dark matter, Phys. Rev. D **62**, 043003 (2000).

[15] T. Aramaki, C. J. Hailey, S. E. Boggs, P. von Doetinchem, H. Fuke, S. I. Mognet, R. A. Ong, K. Perez, and J. Zweerink, Antideuteron sensitivity for the GAPS experiment, Astropart. Phys. **74**, 6 (2016).

[16] T. Aramaki, P. O. H. Adrian, G. Karagiorgi, and H. Odaka, Dual MeV gamma-ray and dark matter observatory—GRAMS Project, Astropart. Phys. **114**, 107 (2020).

[17] T. Aramaki *et al.*, Review of the theoretical and experimental status of dark matter identification with cosmic-ray antideuterons, Phys. Rep. **618**, 1 (2016).

[18] S. Acharya *et al.*, Production of deuterons, tritons, ^{3}He nuclei, and their antinuclei in pp collisions at $\sqrt{s} = 0.9$, 2.76, and 7 TeV, Phys. Rev. C **97**, 024615 (2018).

[19] M. Floris, Hadron yields and the phase diagram of strongly interacting matter, Nucl. Phys. **A931**, 103 (2014).

[20] J. Mitchell *et al.*, The BESS Program, Nucl. Phys. B, Proc. Suppl. **134**, 31 (2004).

[21] A. Yamamoto *et al.*, BESS and its future prospect for polar long duration flights, Adv. Space Res. **30**, 1253 (2002).

[22] Y. Ajima *et al.*, A superconducting solenoidal spectrometer for a balloon-borne experiment, Nucl. Instrum. Methods Phys. Res., Sect. A **443**, 71 (2000).

[23] S. Haino *et al.*, Progress of the BESS Superconducting Spectrometer, Nucl. Instrum. Methods Phys. Res., Sect. A **518**, 167 (2004).

[24] T. Yoshida *et al.*, BESS-polar experiment, Adv. Space Res. **33**, 1755 (2004).

[25] A. Yamamoto *et al.*, Search for primordial antiparticles with BESS, Adv. Space Res. **42**, 442 (2008).

[26] K. Yoshimura *et al.*, BESS-Polar experiment: Progress and future prospects, Adv. Space Res. **42**, 1664 (2008).

[27] K. Abe *et al.*, Measurements of cosmic-ray proton and helium spectra from the bess-polar long-duration balloon flights over Antarctica, Astrophys. J. **822**, 65 (2016).

[28] T. Skwarnicki, A study of the radiative CASCADE transitions between the Upsilon-Prime and Upsilon resonances, Ph.D. thesis, INP, Cracow, 1986.

[29] I. Narsky, Estimation of upper limits using a Poisson statistic, Nucl. Instrum. Methods Phys. Res., Sect. A **450**, 444 (2000).

[30] See Supplemental Material at http://link.aps.org/supplemental/10.1103/PhysRevLett.132.131001, for the energy dependency of each term in the equation for calculating the upper limit on the $\bar{d}$ flux.

[31] A. Cuoco, M. Krämer, and M. Korsmeier, Novel dark matter constraints from antiprotons in light of AMS-02, Phys. Rev. Lett. **118**, 191102 (2017).

[32] F. Donato, N. Fornengo, D. Maurin, P. Salati, and R. Taillet, Antiprotons in cosmic rays from neutralino annihilation, Phys. Rev. D **69**, 063501 (2004).

[33] R. Kappl, A. Reinert, and M. W. Winkler, AMS-02 antiprotons reloaded, J. Cosmol. Astropart. Phys. 10 (2015) 034.

[34] M. Aguilar *et al.*, Precision measurement of the boron to carbon flux ratio in cosmic rays from 1.9 GV to 2.6 TV with the alpha magnetic spectrometer on the international space station, Phys. Rev. Lett. **117**, 231102 (2016).